

Estimation of Surface Heat Fluxes at Field Scale Using Surface Layer Versus Mixed-Layer Atmospheric Variables with Radiometric Temperature Observations

WILLIAM P. KUSTAS

USDA-ARS Hydrology Laboratory, Beltsville, Maryland

JOHN H. PRUEGER

USDA-ARS Soil Tilth Laboratory, Ames, Iowa

KAREN S. HUMES

Department of Geography, University of Oklahoma, Norman, Oklahoma

PATRICK J. STARKS

USDA-ARS Grazinglands Research, El Reno, Oklahoma

(Manuscript received 5 February 1998, in final form 18 May 1998)

ABSTRACT

Radiometric surface temperature observations $T_R(\phi)$, near-surface meteorological/surface energy flux (METFLUX), and atmospheric boundary layer (ABL) data were collected during the Washita '94 Experiment conducted in the Little Washita Experimental Watershed near Chickasha, Oklahoma. The $T_R(\phi)$ measurements were made from ground and aircraft platforms near the METFLUX stations located over vegetated surfaces of varying amounts of cover and over bare soil. Continuous, half-hourly averaged ground-based $T_R(\phi)$ measurements essentially at the point scale were calibrated with periodic ground transect and aircraft-based $T_R(\phi)$ observations at coarser resolutions so that the continuous $T_R(\phi)$ measurements would be representative of surface temperatures at the field scale (i.e., on the order of 10^4 m²). The METFLUX data were collected nominally at 2 m above the surface, while ABL measurements were made in the lower 8–10 km of the atmosphere. The “local” wind speed, u , and air temperature, T_A , from the METFLUX stations, as well as the mixed-layer wind speed, U_M , and potential temperature, Θ_M , were used in a two-source energy balance model for computing fluxes with continuous $T_R(\phi)$ measurements from the various surfaces. Standard Monin–Obukhov surface layer similarity was used with the “local” u and T_A data from the METFLUX stations. Bulk similarity approaches were used with the U_M and Θ_M data referenced either to ABL height or the top of the surface layer. This latter approach of using mixed-layer data to drive model computations for the different sites is similar to the so-called flux-aggregation schemes or methods proposed to account for subgrid variability in atmospheric models, such as the “tile” or “mosaic” approach. There was less agreement between modeled and measured fluxes when using mixed-layer versus local meteorological variables data for driving the model, and the type of bulk formulation used (i.e., whether local or regional surface roughness was used) also had a significant impact on the results. Differences between the flux observations and model predictions using surface layer similarity with local u and T_A data were about 25% on average, while using the bulk formulations with U_M and Θ_M differences averaged about 30%. This larger difference was caused by an increase in biases and scatter between modeled and measured fluxes for some sites. Therefore, computing spatially distributed local-scale fluxes with ABL observations of mixed-layer properties will probably yield less reliable flux predictions than using local meteorological data, if available. Given the uncertainty in flux observations is about 20%, these estimates are still considered reasonable and moreover permit the mapping of spatially distributed surface fluxes at regional scales using a single observation of U_M and Θ_M with high resolution $T_R(\phi)$ data. Such $T_R(\phi)$ observations with a 90-m pixel resolution will be available from the Advanced Spaceborne Thermal Emission and Reflection Radiometer to be launched on NASA's Earth Observing System.

1. Introduction

A two-source energy balance model proposed by Norman et al. (1995) was developed for predicting surface

fluxes over partially vegetated surfaces using as the primary boundary condition radiometric temperature observations, $T_R(\phi)$ (hereafter referred to as N95). Future satellite-based instruments such as the Advanced Spaceborne Thermal Emission and Reflection Radiometer (ASTER) (Tsu et al. 1996), which is part of NASA's Earth Observing System AM-1 (EOS AM-1), will provide spatially distributed maps of $T_R(\phi)$ at 90-m pixel resolution. This is significantly finer than the resolution given by other environmental satellites such as the Na-

Corresponding author address: Dr. William P. Kustas, USDA-ARS Hydrology Laboratory, Building 007 BARC-West, Beltsville, MD 20705-2350.
E-mail: bkustas@hydrolab.arsuda.gov

tional Oceanic and Atmospheric Administration Advanced Very High Resolution Radiometer (NOAA AVHRR) (≈ 1000 -m pixel resolution) and Geostationary Operational Environmental Satellite (GOES) (≈ 8000 -m pixel resolution). By aggregating fluxes estimated at this finer resolution to the AVHRR and GOES pixel size and ultimately to the regional scale, we may be able to improve on soil-vegetation-atmosphere (SVAT) aggregation schemes for estimating "effective" model parameters (Raupach and Finnigan 1995). However, to use ASTER data for computing spatially distributed fluxes at this higher resolution, a technique for specifying the atmospheric forcing variables for several adjacent pixels would be required, especially when the surface vegetation cover is significantly heterogeneous at length scales on the order of 10^2 – 10^3 m. At these scales of variability, different surfaces, such as dry bare soil versus a well-irrigated crop, result in significant differences in local meteorological conditions.

Gao (1995) developed a physically based technique from concepts in Seth et al. (1994) for distributing mean meteorological variables from a large-scale atmospheric model to subgrid pixels based on remotely sensed data and concepts from flux footprint theory (Schuepp et al. 1990). A similar approach was developed by Kustas and Humes (1996), but only for wind speed, u . Unfortunately, variations in air temperature, T_A , can have a significant effect on N95 model flux predictions (Anderson et al. 1997; Kustas and Norman 1997; Zhan et al. 1996). For example, Gao et al. (1998) found variations in T_A reaching 3° – 4°C for a NOAA AVHRR scene over a region in the Southern Great Plains, thus requiring a technique for estimating the spatial distribution of T_A . Other studies have found that under certain environmental conditions, the spatial variability of u and $T_R(\phi)$ can have a more significant affect on computed fluxes than T_A (Qualls and Brutsaert 1996).

A much simpler scheme of dealing with subgrid variability (e.g., vegetation variations within a large-scale atmospheric model grid) or subpixel variability (e.g., using ASTER instead of GOES data for computing spatially distributed fluxes over a region), which takes full advantage of the spatial information available from remotely sensed observations, is the "mosaic" or "tile" approach (Avisar and Pielke 1989; Koster and Suarez 1992). In this scheme, specific surface types are defined and weighted by the fractional area they occupy within each large-scale atmospheric model grid and an area-weighted flux is derived using mean grid cell atmospheric forcing variables. This concept was applied to experimental data analyzed by Mahrt and Sun (1995), who found that using spatially constant atmospheric variables with spatially varying surface conditions satisfactorily reproduced the area-average heat flux for three different surfaces.

In the case of the Little Washita Experimental Watershed, the scale of surface heterogeneity is on the order of 10^2 – 10^3 m resembling a type A surface as defined

by Shuttleworth (1988) and Claussen (1995). For this type of surface, Blyth et al. (1993) and Claussen (1991) show the so-called tile or flux-aggregation approach is applicable but that the atmospheric variables should be defined at the blending height where wind speed and scalars can be treated as uniform over the landscape (Mason 1988). Blyth (1995) shows how the blending height principle can be modeled simply for a mixture of two surfaces. However, when the region is an agricultural patchwork of surfaces containing a wide range of fractional vegetation cover, it is not readily apparent how the blending height method can be applied.

Mahrt (1996) indicates that for a type A surface, atmospheric conditions are likely to be horizontally homogeneous at the top of the surface layer, even in the presence of small-scale mesoscale surface variations (see also Claussen 1995; Raupach and Finnigan 1995). This is supported by a large-eddy simulation (LES) study of Hechtel et al. (1990) in which the LES was applied to a type A surface using observations from the 1983 boundary layer experiment conducted over a region covering the Little Washita watershed (Stull and Eloranta 1984). Therefore, even though at the local or field scale there will be variations in u and T_A not considered in model computations, spatially distributed fluxes estimated using bulk atmospheric boundary layer (ABL) formulations (e.g., Brutsaert and Sugita 1991) may provide acceptable estimates. Such an approach was applied by Kustas and Humes (1996) over a semi-arid rangeland site and was shown to give very similar results to assigning a spatially variable wind speed to each pixel.

In this paper, continuous $T_R(\phi)$ observations representative of spatial scales on the order of 10^0 m² and timescales 10^3 s are compared to observations collected at resolutions of 10^3 – 10^4 m² and 10^0 – 10^2 s for four fields ranging from no vegetation (bare soil) to nearly full cover. The continuous $T_R(\phi)$ observations are used with an N95 two-source model with several modifications (see below).

The reliability of the two-source model predictions of the heat fluxes using the "local" meteorological data, u and T_A , is evaluated using flux observations obtained from eddy covariance and Bowen ratio methods. The ABL observations are then used to define mixed-layer wind speed, U_M , and mixed-layer potential temperature, Θ_M , and are employed in bulk ABL formulations for computing the "field-" or "local-" scale fluxes for the four sites. These estimates are compared with the flux observations and the N95 model results using the field or local scale u and T_A data. Since the heat fluxes estimated using surface layer and mixed-layer atmospheric data are affected by local versus "regional-scale" processes, respectively, this study provides unique observational evidence of the utility in the mosaic or tile approach applied to type A surfaces with high-resolution remote sensing data.

2. The data

a. The field experiment

The Washita '94 experiment took place in the Little Washita river basin (34.8°N, 98.2°W) near Chickasha, Oklahoma. The basin is approximately 610 km² in area and drains into the Washita River. The terrain is a mildly hilly mixture of rangeland, pasture, and cropland with smaller areas of forests, urban areas, highways, oil waste land, quarries and reservoirs (Allen and Naney 1991). The Washita '94 experiment was a cooperative effort between USDA, NASA, and several other government agencies and universities. The main objective of the experiment was to combine ground and remotely sensed data for quantifying surface energy and hydrologic fluxes at basin scales. The types of ground-, aircraft- and satellite-based remote sensing data, and hydrologic and meteorological data are summarized in a data report (Starks and Humes 1996).

One of the intensive data collection campaigns covered the period from 17 August through 23 August 1994, or day of year (DOY) 229–235. In the beginning of the field campaign (DOY 229–231) there were several rain events resulting in approximately 30 mm of cumulative precipitation being recorded by many of the rain gauges in the watershed. The only other precipitation fell as light rain on DOY 232–233, which amounted to less than 2 mm. At the start of the observations, the soil surface across the basin was fairly wet. With no significant rain events occurring after the morning of DOY 231, some drying of the near-surface soil occurred for DOY 232–235.

b. Micrometeorological data

Micrometeorological data were collected at four sites during the August field campaign. The observations at the meteorological/surface energy flux (METFLUX) stations included meteorological variables at a nominal 2-m height, that is, wind speed (u), air temperature (T_A), vapor pressure (e_A), solar radiation (R_{sol}), and measurements of soil heat flux (G), net radiation (R_N), and the turbulent fluxes of sensible (H) and latent (LE) heat. The variables H and LE were estimated at three of the sites with one-dimensional eddy correlation (covariance) systems composed of a Campbell Scientific¹ CA27 sonic anemometer with a fine-wire thermocouple and a KH20 krypton hygrometer. A Bowen ratio system manufactured by Radiation and Energy Balance Systems (REBS) was used at the other location. All measurements were averaged on a half-hourly basis. Net radiation was estimated with a REBS Q*7 net radiometer. Soil heat flux was estimated using several REBS HFT-

3 soil heat flux plates buried at 0.08 m and heat storage above the plates computed with soil temperature measurements at depths of 0.02 and 0.06 m (Brutsaert 1982). The surface flux measurements are discussed in Prueger et al. (1996a) and Prueger et al. (1996b).

The estimates of R_N made with the REBS Q*7 net radiometers during the experiment had to be adjusted due to errors discovered by REBS in the original calibration procedure of the sensors and sensitivity to wind speed (C.B. Fritschen 1997, personal communication). The nominal values of the calibration coefficients of the REBS Q*7 net radiometers had to be increased by approximately 16%, and a wind correction algorithm suggested by REBS increased these measured values by an additional 4%–5%. Thus, the original net radiation values were increased by approximately 20%. Net radiation was also calculated by an approach summarized in Kustas et al. (1995). This uses the observed R_{sol} and an estimate of the shortwave albedo based on surface cover from Brutsaert (1982) for computing the net shortwave radiation balance. The net longwave radiation balance is estimated using T_A and e_A for estimating atmospheric longwave (see Brutsaert 1982) and $T_R(\phi)$ observations for computing the surface longwave radiation. The computed values were about 17% higher on average than the original net radiation observations, providing support for the adjustment.

Studies comparing eddy covariance and Bowen ratio techniques for estimating H and LE typically find variations on the order of 20% for agricultural and natural surfaces (e.g., Dugas et al. 1991; Fritschen et al. 1992; Nie and coauthors, 1992). A common method for gaining confidence in the eddy covariance estimates of the heat fluxes is to evaluate how closely $H + LE = R_N - G$. Studies have found with eddy covariance measurement of the heat fluxes that $H + LE$ is generally less than $R_N - G$ during daytime conditions (Stannard et al. 1994). When expressed as a ratio, namely, the closure ratio $CR = (H + LE)/(R_N - G)$, values of CR typically range between 0.8 and 0.9 for agricultural crops, although values as low as 0.7 have been reported (Kizer and Elliot 1991). The average daytime value of CR for the three sites was approximately 0.77, indicating about 20% of the available energy, $R_N - G$, is not accounted for by the eddy covariance measurements. There are obviously measurement uncertainties in R_N and G ; however, it is unlikely that the errors in G for all the sites would consistently cause a larger available energy term to be computed. Furthermore, the magnitude of G relative to R_N was usually small. Generally, G was less than 10% of R_N for the vegetated sites and about 25% of R_N for the bare soil site during the daytime. Increasing the original R_N observation by 20% may be an overestimate of the adjustment required; yet, the calculated R_N values were within 5% of the adjusted. This provides some confidence in the correction applied to the R_N data. Since the model assumes $R_N - G - H - LE = 0$ [cf. Eq. (A5)], and in the present study the model used the

¹ Company and trade names are given for the benefit of the reader and imply no endorsement by the USDA.

R_N observations as input for determining the available energy of the soil and vegetation [cf. Eqs. (A6) and (A7)], the eddy covariance measurements of the heat fluxes were also forced to have a closure equal to zero. To satisfy a zero closure, but preserve the relative partitioning of the available energy between H and LE, the value of the Bowen ratio (i.e., $B_o = H/LE$) from the eddy covariance measurements was used in Eq. (A5) for recomputing the H and LE fluxes. This resulted in an average increase in the observed H of about 45 W m^{-2} and an average increase in the observed LE of about 55 W m^{-2} .

The zero closure adjustment to the eddy covariance measurements of H and LE assumes that the available energy term $R_N - G$ is without error and that all the error is caused by the inability of the eddy covariance technique to measure all the turbulent eddies contributing to the heat fluxes. The undermeasurement of the turbulent fluxes by eddy covariance is well documented (e.g., Kizer and Elliot 1991), but there are also studies indicating significant uncertainty in measuring the available energy term (e.g., Stannard et al. 1994). Unfortunately, errors in R_N and G cannot be easily quantified since these measurements were not replicated at each site, and even if they were, it is not obvious how to assign error terms to R_N and G . There are indications that the uncertainty in the estimates of the available energy term is about 10% since differences between the “corrected” and calculated R_N for individual sites were within 5% and, for at least the vegetated sites, G is a relatively minor component.

Energy balance models require $R_N - G - H - LE = 0$, as well as the Bowen ratio technique for estimating H and LE. Therefore, the zero closure adjustment to the original eddy covariance measurements of H and LE forces the measurements to be consistent with the model requirement of energy conservation; it also results in the adjusted fluxes being consistent with the site using the Bowen ratio technique. Furthermore, by using B_o estimated from the original eddy covariance observations of H and LE to force closure, this adjustment preserves the original estimates of the relative partitioning of available energy between H and LE by the eddy covariance systems.

Since energy conservation is imposed on both modeled and measured heat fluxes, discrepancies between model-predicted and measured H and LE fluxes is mainly correlated to differences between model and observed B_o . This will more likely result in differences between modeled and observed heat fluxes having a significant nonrandom or bias component, if the model is well behaved. This bias may be more easily related to values of model parameters and variables prescribed for a given site.

c. Atmospheric boundary layer data

Atmospheric soundings were conducted approximately in the center of the watershed on a site approx-

imately 435 m above mean sea level (MSL) with panoramic views of the watershed in all directions. The sounding data were collected with a Mobile Cross-Chain Loran Atmospheric Sounding System (M-CLASS; Rust et al. 1990). The M-CLASS uses a Väisälä RLS-80 sonde, which receives Loran navigation in order to track the balloon for estimating horizontal wind speed and direction. Pressure, temperature, and humidity data are sent to the ground station for collection and processing. Further details of the ABL sounding system and measurements during Washita '94 can be found in the data report (Ziegler and Showell 1996).

Soundings were conducted at the nominal times of 0500, 0800, 1100, 1400, and 1700 central standard time (CST), which corresponds to 1100, 1400, 1700, 2000, and 2300 UTC. Geopotential height was computed using the hypsometric equation with range, azimuth, and elevation of the sonde obtained from the Loran data. Air temperature, relative humidity, wind speed, and direction were available every 30–50 m up to an altitude of approximately 8000 m MSL. Ziegler and Showell (1996) provide a mesoscale weather summary table that indicated that mesoscale activity causing precipitation and unstable weather conditions existed for DOY 230–232 with a cold frontal passage on the morning of DOY 232.

d. Remote sensing data

The remote sensing data used in this study came from ground and aircraft platforms that supported thermal infrared radiometers (IRTs), manufactured by Everest Interscience, which have a bandpass of approximately 8–13 μm . Continuous observations (half-hourly averages) of $T_R(\phi)$ were made at each of the micrometeorological stations with a nadir-viewing fixed-head IRT (Model 4000) mounted approximately 1.5 m above ground level (AGL). The IRTs had a 60° field of view (FOV), which meant that the sensor integrated over a surface area approximately 1.5 m in diameter.

Ground-based IRT data were also collected using a backpack-type apparatus (called a yoke) supporting a nadir-viewing IRT (Model 110/130) with a 15° FOV at approximately 2 m AGL. A single observation represented a pixel approximately 0.5 m in diameter. With a set of ground transects, this measurement system permitted the collection of $T_R(\phi)$ data over a relatively large area in a short amount of time. Such a system has been used in a number of previous field studies (e.g., Moran et al. 1994). Data were acquired at different sites on different days. The area covered at each site varied from 0.6 to 2 ha, depending on the uniformity of the land surface with the measurements made upwind of the flux measurement station (typically south to southwest). Each traverse consisted of a set of repeatable transects having a grid-type pattern. They were covered in both the “forward” and “reverse” directions with the whole traverse taking roughly 10–15 min to com-

TABLE 1. Description of surface conditions and surface cover information for the four METFLUX sites.

Site	Dominant species	General condition	h_c/h_o^a (m)	LAI ^b	f_c^c	f_G^d
1	Buffalograss (<i>Buchloe dactyloides</i>), Little Bluestem (<i>Schizachyrium scoparium</i> var <i>frequens</i>), and Switchgrass (<i>Panicum virgatum</i>)	Lightly grazed	0.5	2.5	0.80	0.65
2	Bermuda grass (<i>Cynodon dactylon</i>)	Recently harvested	0.1	1	0.50	0.90
3	Bermuda grass (<i>Cynodon dactylon</i>)	Heavily grazed	0.15	1.5	0.65	0.80
4	N/A	Plowed wheat stubble/bare soil	0.1	N/A	N/A	N/A

^a h_c is the mean canopy or vegetation height and h_o is the mean obstacle height (i.e., height of the bare soil clods/wheat stubble).

^b LAI is the leaf area index.

^c f_c is the fractional canopy or vegetation cover.

^d f_G is the fraction of vegetation that is green.

plete, depending on the size. Approximately 30 data points were collected for each 30 m of transect with anywhere from 150 to nearly 400 data points in total being acquired for a measurement sequence. For a given site, a traverse was performed every hour, approximately, from about 0900 to 1700 CST.

A third set of $T_R(\phi)$ observations were acquired from a low-flying aircraft with a nadir-viewing 15° FOV IRT (Model 110) at approximately 100–150 m AGL, thus producing pixels of 25–40 m in diameter. The aircraft flew several transects 10–20 km in length over the watershed both in a forward and reverse modes and typically flew over the flux stations twice, once in a north–south and then a south–north direction. Measurements were acquired at 1 Hz so that with the aircraft speed of approximately 100 m s⁻¹ a set of five measurements traversed over an area on the order of 500 m in length. The aircraft data contained a video system and a global positioning system unit so that the data were georegistered to known ground locations, including the METFLUX stations.

In summary, the $T_R(\phi)$ observations represented areas with length scales of 10⁰–10² m and temporal scales from essentially “instantaneous” to half-hourly averaged values from the continuous observations (i.e., 10⁰–10³ s). In essence, the $T_R(\phi)$ observations having the largest spatial scale have the shortest timescale (i.e., aircraft measurements), while the longest timescale observation of $T_R(\phi)$ comes from the highest spatial resolution observations, namely, the fixed-head IRT sensors mounted at the METFLUX sites.

e. Site description

Table 1 contains a description of the vegetation cover and general surface conditions of the four METFLUX sites where the micrometeorological data were collected. Site 1 can be described as native pasture with relatively dense cover of several grass species including

Buffalograss (*Buchloe dactyloides*), Little Bluestem (*Schizachyrium scoparium* var *frequens*), and Switchgrass (*Panicum virgatum*) interspersed with several forbes. Site 2 was a Bermuda grass (*Cynodon dactylon*) pasture of marginal quality that was recently harvested, while site 3 was an improved Bermuda grass pasture heavily grazed by cattle. Site 4 was a recently harvested and plowed wheat field containing 5–10-cm-diameter soil clods and a significant amount of wheat stubble. The four sites were located in fields ranging in size from 35 to 5 ha. Sites 1, 3, and 4 had good fetch conditions with dimensions of 200–500 m in the east–west and 800–1000 m in the north–south directions. On the other hand, site 2 had marginal fetch with nominal dimensions of 160 m east–west and 300 m north–south. Fortunately, most days had southerly winds, maximizing fetch for all sites except on DOY 233; here the winds were predominately from the east.

To estimate the leaf area index (LAI) for sites 1–3 fractional vegetation cover f_c was first estimated from nadir photos taken 2 m above the surface near the flux stations. The photos were overlaid with 10 × 15 cm grid containing 600 points (i.e., each grid box was 0.5 × 0.5 cm). Estimates of f_c were approximately 80%, 50%, and 65% for sites 1, 2, and 3. For relatively homogeneous canopies there is an exponential relationship between f_c and LAI (Choudhury 1987):

$$f_c = 1 - \exp(-\beta \text{LAI}), \quad (1)$$

where β is a function of the leaf angle distribution (e.g., $\beta = 0.5$ for randomly distributed leaves). Choudhury et al. (1994) estimated a mean $\beta = 0.67$ from β values for 18 crops presented by Ross (1975). With the estimates of f_c in Table 1, this yields LAI values of approximately 2.5, 1, and 1.5 for sites 1, 2, and 3, respectively. The photos also indicated that sites 1 and 3 contained a significant fraction of senescent vegetation. This will affect model flux predictions since the model formulation of canopy transpiration [i.e., Eq. (A14) in

the appendix] is only appropriate for the green fraction of the vegetation, f_G . Estimates were $f_G = 0.65, 0.90,$ and 0.80 for sites 1, 2, and 3, respectively. Normally it is assumed that $f_G \approx 1$, so the impact of this departure from unity on model results will be discussed later.

3. Model description

Details of the two-source N95 model are given in Norman et al. (1995) and Kustas and Norman (1997). A brief description of the model formulations is given in the appendix. There are three modifications to the original version of the model that will be discussed here. The first two revisions to the N95 model have to do with accounting for the temporal variation in net radiation partitioning between the vegetation and soil surface and the time-dependent variation of the soil heat flux–net radiation relationship.

In the original version of the model, the exponential extinction of net radiation R_N through the canopy was assumed to be constant over the course of the day. A modification recently proposed by Anderson et al. (1997) is used based on simulations with a detailed soil–plant–atmosphere model, Cupid (Norman and Campbell 1983). In this case an additional term is included as a function of solar zenith angle so that the net radiation at the soil surface, R_{NS} , and absorbed by the canopy, R_{NC} , are estimated by the following:

$$R_{NS} = R_N \exp\{-\kappa LAI/[2 \cos(\theta_s)]^{1/2}\} \quad (2a)$$

and

$$R_{NC} = R_N(1 - \exp\{-\kappa LAI/[2 \cos(\theta_s)]^{1/2}\}), \quad (2b)$$

where $\kappa = 0.6$ is used so that at high solar zenith angle elevations (i.e., $\theta_s < 30^\circ$) the quantity $\kappa(2 \cos\theta)^{-1/2}$ will have a value of about 0.45, which is midway between its likely limits of 0.3–0.6 (Ross 1981). The second modification is in the estimate of the soil heat flux G . For computing G , the original formulation from N95 is simply

$$G = c_G R_{NS}, \quad (3)$$

where the value of c_G ranges from 0.2 to 0.5 (Choudhury et al. 1987). However, assuming c_G is constant is valid only for several hours around solar noon (Kustas and Daughtry 1990), and studies (e.g., Friedl 1996) also indicate that it may vary with soil conditions (e.g., soil moisture). Friedl (1996) included the effects of a temporally varying c_G by multiplying Eq. (3) by $\cos(\theta_s)$. Another approach developed by Kustas et al. (1998) is based on time differences with the local solar noon quantified by the following nondimensional time parameter t_N ,

$$t_N = \frac{|t_i - t_{SN}|}{t_{SN}}, \quad (4)$$

where t_i is the time nominally plus or minus 5 h of the local time of solar noon, t_{SN} (≈ 1245 LST), and $||$ rep-

resents the absolute value of the difference. Using experimental data to compute G/R_{NS} or c_G as a function of time t_i , an empirical function was fit between G/R_{NS} and t_N . The results indicated that a constant G/R_{NS} could be used for $t_N < 0.3$ (i.e., several hours around solar noon) and linear least squares regression equation between G/R_{NS} and t_N was needed for $t_N > 0.3$. Neither Eq. (4) nor the approach suggested by Friedl (1996), however, considers the fact that G and R_N are not in phase, and, hence, the temporal change in the ratio G/R_{NS} will not be the same between the morning and afternoon.

The third modification has to do with changing how the aerodynamic resistance between the surface and the mixed layer or the top of the surface layer is parameterized. For the bulk similarity approach with U_M and Θ_M the resistance R_{AH} and R_A have the following form:

$$R_{AH} = \frac{\left[\ln\left(\frac{z_{ABL} - d_o}{z_{OM}}\right) - B_M \right] \left[\ln\left(\frac{z_{ABL} - d_o}{z_{OH}}\right) - C_H \right]}{k^2 U_M} \quad (5a)$$

and

$$R_A = \frac{\left[\ln\left(\frac{z_{ABL} - d_o}{z_{OM}}\right) - B_M \right] \left[\ln\left(\frac{z_{ABL} - d_o}{z_{OM}}\right) - C_H \right]}{k^2 U_M}, \quad (5b)$$

where z_{ABL} is the inversion height, which is essentially the height of the mixed layer; k is von Kármán's constant; and B_M and C_H are the bulk similarity stability correction functions for momentum and heat, respectively. A summary of different formulations for B_M and C_H is given by Sugita and Brutsaert (1992). The following were used based on results from Kustas et al. (1995):

$$B_M = 0.4 \ln \left[\frac{-(z_{ABL} - d_o)}{L} \right] + 4.4 \quad (6a)$$

and

$$C_H = 0.54 \ln \left[\frac{-(z_{ABL} - d_o)}{L} \right] + 2.3, \quad (6b)$$

where L is the Monin–Obukhov length (see the appendix). Kustas and Humes (1996) also applied U_M and Θ_M with Eq. (A4) and z taken at the top of the surface layer, z_{SL} , assumed to be about 50 m (Raupach and Finnigan 1995), along with using the improved surface layer stability correction functions for Ψ_M proposed by Brutsaert (1992) and the original Businger–Dyer function for Ψ_H for unstable conditions. Kustas and Humes (1996) found sensitivity of model output to various ways of estimating z_{SL} , such as 10% of z_{ABL} was negligible. The use of U_M and Θ_M with standard surface layer formulations for Ψ_M and Ψ_H is not supported theoretically by matching the inner and the outer regions of the ABL (Brutsaert and

Sugita 1991). However, it is considered a reasonable approximation since Sugita and Brutsaert (1992) show that by matching these two regions, Ψ_H and Ψ_M are used in predicting C_H and B_M (see below).

With the so-called tile or flux-aggregation approach, the roughness parameters z_{OM} , d_o , and z_{OH} of the local or “elemental area” is used, which is commensurate with the surface temperature of the elemental area (Rau-pach and Finnigan 1995). The local roughness values are representative of the bare soil and grass-covered surfaces that affect local u and T_A . However, at regional scales, ABL flow is affected by “regional” roughness values Z_{OM} , D_o , and Z_{OH} , similar to the “effective” roughness discussed by Mason (1988). These roughness values are representative of upwind fetches on the order of 10^0 – 10^1 km, which affect regional shear stress and hence U_M (Brutsaert and Parlange 1996). By using regional roughness values and matching surface layer and mixed-layer resistances R_{AH} and R_A , Sugita and Brutsaert (1992) developed bulk stability correction functions that remove the explicit dependence upon z_{ABL} . The expressions for B_M and C_H have the form

$$B_M = \Psi_M \left[\frac{c_1 Z_{OM}}{L} \right] + \ln \left[\frac{(z_{ABL} - D_o)}{Z_{OM}} \right] - c_2 \quad (7a)$$

and

$$C_H = \Psi_H \left[\frac{c_3 Z_{OM}}{L} \right] + \ln \left[\frac{(z_{ABL} - D_o)}{Z_{OM}} \right] - c_4, \quad (7b)$$

where the improved surface layer stability correction functions for Ψ_M proposed by Brutsaert (1992) and the original Businger–Dyer function for Ψ_H for unstable conditions are used, as are the constants $c_1 = c_3 \approx 70$, $c_2 \approx 4.3$, and $c_4 \approx 4.8$ (Sugita and Brutsaert 1992). When Eqs. (7a) and (7b) are substituted into Eqs. (5a) and (5b) with regional roughness values Z_{OM} , D_o , and Z_{OH} , the $\ln[(z_{ABL} - D_o)/Z_{OM}]$ term is factored out removing the explicit dependence upon z_{ABL} . The impact on model results using regional roughness values will be discussed below. Application of Eqs. (5a) and (5b) with either z_{ABL} or z_{SL} requires that the potential temperatures of the canopy Θ_c , soil Θ_s , and the canopy air space Θ_{AC} be used in Eqs. (A8)–(A12) with Θ_M replacing T_A .

4. Results and discussion

a. Surface temperature data used in the model

Comparisons between the fixed-head and yoke IRT observations and between the fixed-head and aircraft IRT observations for all four sites indicated differences were typically less than 1°C . The half-hourly averaged fixed-head IRT values were interpolated to match the time of the yoke and aircraft-based $T_R(\phi)$ observations. Estimates of $T_R(\phi)$ from the aircraft were an average of five observations (± 2 pixels from the one determined

as the closest to the actual METFLUX station). This gave an average $T_R(\phi)$ of which the length scale is representative of the fetch or source area contributing to the flux observations made at about 2 m (Schuepp et al. 1990).

The root-mean-square difference (rmsd; Willmott 1982) values as well as the standard errors (SEs) of the least squares regression between fixed-head IRT and the yoke and aircraft measurements were about 2°C and 1°C , respectively, except at site 2. The aircraft $T_R(\phi)$ observations suggested that with less vegetation and more exposed bare soil cover at site 2, this caused more variability in surface temperature. Thus for site 2, a time-dependent correction factor was used that yielded a comparable SE (i.e., $\approx 1^\circ\text{C}$) with the other sites. There were only a few cases where yoke and aircraft IRT observations could be compared. The resulting rmsd of about 1.6°C between the yoke and aircraft-derived $T_R(\phi)$ is similar in magnitude to rmsd value between fixed-head and aircraft IRT data.

The yoke data were considered the most reliable for two reasons: 1) the average value of $T_R(\phi)$ represented over 150 “instantaneous” measurements collected over a 10–15-min duration, which is comparable to the averaging time of the flux and meteorological observations, and 2) these data were collected over about 10^2 m² areas, which is the same order of magnitude as the source area affecting the METFLUX observations. The fixed-head IRT observations afforded the maximum number of model comparisons with the flux measurements. Therefore, these data were calibrated using least squares regression equations with the yoke data as the dependent variable for sites 1, 3, and 4. For site 2, the fixed-head IRT data were calibrated using the time-dependent formulation.

b. Meteorological data used in the model

The model was run using u and T_A data from each site available on a half-hourly basis. Data for the three days (i.e., DOY 233–235) following unsteady weather conditions were used for running the model and evaluating flux predictions. The ABL data were only available every 3 h. Estimates of U_M and Θ_M were determined from plotting the Θ profiles and estimating the height of the inversion; this typically ranged between 50 and 2000 m AGL. All Θ and U values over this depth were then averaged to give an estimate of U_M and Θ_M . Mixed-layer depths were well defined for the 1100, 1400, and 1700 CST soundings. For the 0800 CST sounding, the inversion height was close to the surface, thus a mixed layer was not well defined; it was assumed to be 50 m in depth. To have U_M and Θ_M values for each half-hourly $T_R(\phi)$ observation, a linear interpolation was used between sequential soundings for predicting the time rate change of U_M , Θ_M , and z_{ABL} .

TABLE 2. Description of the four versions of the N95 model used in computing heat fluxes for the four METFLUX sites.

Model version	Description
N95 _L	Uses local wind speed u and air temperature T_A observations from each METFLUX site with N95 formulations in the appendix and modifications described in the text.
N95 _{BL}	Uses mixed-layer wind speed U_M and potential temperature Θ_M . Replaces Eq. (A4) with Eqs. (5b), (6a), and (6b), and $z_{OH} = z_{OM}$ and with the height of the ABL, z_{ABL} , as the reference height for estimating R_A .
N95 _{SL}	Uses mixed-layer wind speed U_M and potential temperature Θ_M . Uses Eq. (A4) and $z_{OH} = z_{OM}$, and with the top of the surface layer $z_{SL} = 50$ m, as the reference height for estimating R_A .
N95 _{SB}	Uses mixed-layer wind speed U_M and potential temperature Θ_M . Replaces Eq. (A4) with Eqs. (5b), (7a), and (7b) from Sugita and Brutsaert (1992) and uses regional roughness Z_{OM} instead of the local roughness z_{OM} with $Z_{OH} = Z_{OM}$ for estimating R_A .

c. Model results using local meteorological and ABL data

The N95 model described in the appendix uses both a “parallel” versus “series” resistance network for computing H_s and H_c [i.e., Eqs. (A8) and (A9) versus Eqs. (A10) and (A11), respectively]. Although predicted fluxes were similar using either resistance network, N95 suggests that the series version is better suited for more closed canopies where there is a stronger interaction between soil and canopy (see also in N95, Figs. 1 and 11 illustrating the parallel and series resistance network). Therefore in this paper, flux predictions with N95 model using the series resistance network will only be compared to the observations.

Four versions of N95 model were evaluated and are summarized in Table 2. One version used local meteorological data u and T_A data collected at 2 m from each site with the N95 model summarized in the appendix (N95_L). The other three versions of the N95 model employed values of U_M and Θ_M . Two versions used either z_{ABL} or z_{SL} with the corresponding bulk layer (N95_{BL}) or surface layer (N95_{SL}) stability correction functions, respectively. The other model version (N95_{SB}) was also run using the bulk similarity approach but with the stability functions for B_M and C_H developed by Sugita and Brutsaert (1992) [cf. Eqs. (7a) and (7b)] and with a regional roughness of $Z_{OM} \approx 0.3$ m (Beljaars 1995) instead of z_{OM} values assigned to each elemental area, which were an order of magnitude smaller. When using Eq. (5a) with the parallel version of the model, Z_{OH} also needs to be specified. However, with the series version an explicit value for Z_{OH} is not required (see the appendix). Results from N95_{BL}, N95_{SL}, and N95_{SB} are presented for only H and LE fluxes since there were negligible changes in the model estimates of G from N95_L.

1) RESULTS USING LOCAL METEOROLOGICAL DATA

Comparisons of predicted versus observed H , LE, and G using local meteorological data with the N95 model, N95_L, are shown in Fig. 1. In general, model performance in predicting the fluxes appears satisfactory, but

for some sites (particularly sites 1 and 2) the model has a tendency to either over- or underpredict H , which typically causes the opposite result with the LE predictions. Differences between model and observed fluxes were quantified using rmsd and the mean-absolute-percent difference (mapd), which is the average of the absolute differences between model and measured fluxes divided by the measured flux (see Table 3). The mapd values were not computed for several periods when measurements averaged less than 10 W m^{-2} . By computing mapd values, model performance can be more easily compared to typical flux measurement uncertainties (see below).

In Table 3, the results using the N95_L model with the parameters listed in Table 1 and with $f_G = 1$ are listed. From using $f_G = 1$, both rmsd and mapd increase by approximately $10\text{--}20 \text{ W m}^{-2}$ and approximately 5%, respectively, suggesting that having a reliable estimate of f_G when it is significantly less than one (i.e., sites 1 and 3) is important. In fact, a sensitivity analysis by Kustas and Norman (1997) indicates that a 20% change in f_G can cause a similar change in predicted H . The uncertainty in half-hourly or hourly turbulent flux observations over prairie grasslands using eddy covariance and Bowen ratio techniques is typically 20% (Fritschen et al. 1992; Kustas and Norman 1997). For G , the uncertainty is larger, probably more on the order of 30% (Stannard et al. 1994). Thus differences between model and observed H and LE fluxes averaging 15%–25% are comparable to the uncertainty in measurement techniques. The relatively larger difference found with G (where mapd $\approx 30\%$) is marginally acceptable.

2) RESULTS USING ABL DATA

The statistical results in Table 4 show a general increase in both rmsd and mapd when using the N95 model with U_M and Θ_M and similarity for estimating the fluxes over the various surfaces (i.e., the tile approach). The magnitudes of rmsd and mapd indicate the N95 model's performance in predicting H and LE is still satisfactory (i.e., within the level of uncertainty in the flux measurement

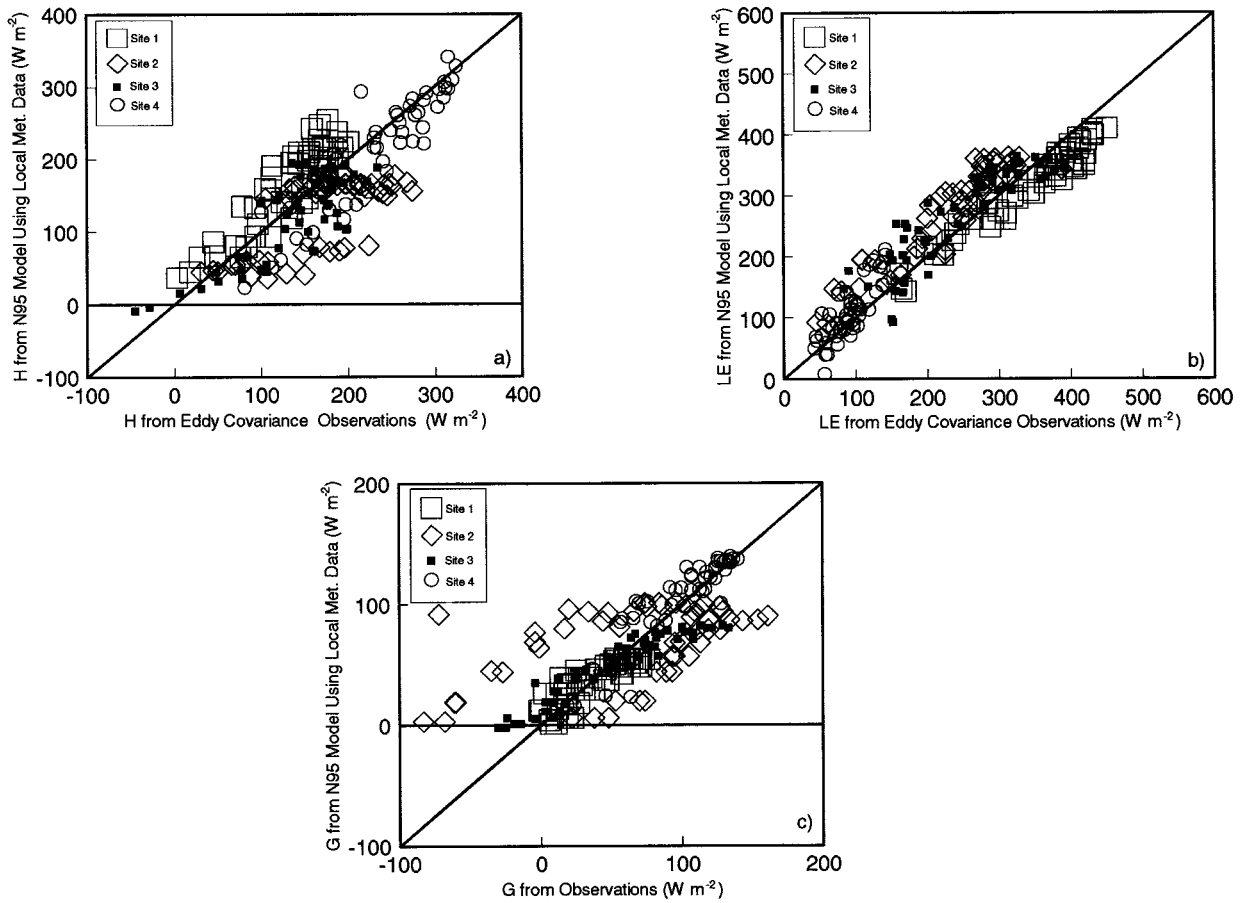


FIG. 1. N95_L model predictions of (a) H , (b) LE , and (c) G using a variable f_G vs the flux observations from the METFLUX sites. See text and Table 2 for a description of the N95_L model version. The lines represent perfect agreement.

techniques) when using the bulk layer N95_{BL} and surface layer N95_{SL} similarity approaches with z_{OM} values. However, the results are generally unsatisfactory in predicting the heat fluxes when using regional roughness, Z_{OM} , and stability functions suggested by Sugita and Brutsaert (1992) in Eq. (5b), N95_{SB}. The predicted heat fluxes using N95_{BL} and N95_{SL} were very similar. Therefore, comparisons between predicted and observed heat fluxes for individual sites are illustrated for only N95_{BL} (Fig. 2). The increase differences with the observed fluxes compared to

N95_L are mainly seen as an overall increase in bias in the flux predictions for some of the sites. For example, notice that the predicted heat fluxes for site 4 fall further away from the 1:1 line in Fig. 2 than in Fig. 1. For N95_{SB}, there is not only larger biases in heat flux predictions for most of the sites but also considerably more variability or scatter (Fig. 2).

A final comparison is shown between H and LE predicted by N95_L and the other approaches (Fig. 3). Since the results with N95_{BL} and N95_{SL} were very similar, only

TABLE 3. Statistical results comparing N95_L model-predicted H , LE , and G with variable f_G ($f_G < 1$) and f_G assumed to equal unity ($f_G = 1$).

Model assumption for f_G	rmsd* for H (W m ⁻²)	rmsd for LE (W m ⁻²)	rmsd for G (W m ⁻²)	mapd** for H (%)	mapd for LE (%)	mapd for G (%)
$f_G < 1$	47	41	30	25	20	29
$f_G = 1$	58	56	30	33	25	29

* rmsd is the root-mean-square difference, which is the square root of the sum of the squared differences between modeled and observed divided by the number of samples (see Wilcott 1982).

** mapd is the mean-absolute-percent difference, which is the average of absolute differences between model and measured fluxes divided by the measured flux.

TABLE 4. Statistics for N95_L model version and N95 versions using mixed-layer variables Θ_M and U_M with bulk and surface layer similarity approaches, namely, N95_{BL}, N95_{SL}, and N95_{SB} (see Table 2).

Model version	rmsd H ($W m^{-2}$)	rmsd LE ($W m^{-2}$)	mapd H (%)	mapd LE (%)
N95 _L	47	41	25	20
N95 _{BL}	51	46	29	23
N95 _{SL}	53	48	29	26
N95 _{SB}	84	89	46	37

N95_{BL} model predictions are compared to N95_L. In Fig. 3, symbols are not used to distinguish estimates from the different sites. The N95_{BL} predictions tend to underestimate H when $H > 200 W m^{-2}$ and overestimate LE when $LE < 200 W m^{-2}$. The agreement with N95_L, however, is quite good with mapd $\approx 10\%$ for H and $\approx 15\%$ for LE. For N95_{SB}, there is a general tendency to overestimate H and hence underestimate LE along with significantly more scatter. This results in larger mapd values between N95_{SB} and N95_L predictions with mapd $\approx 55\%$ for H and 35% for LE.

To minimize errors caused by the interpolation scheme used in estimating half-hourly values of U_M and Θ_M between soundings, the model was also run only for the two half-hourly values surrounding the time of the 1100 and 1400 CST soundings. The rmsd values between predicted and observed heat fluxes were similar to the values listed in Table 4, while the mapd values were generally lower. This is due in part to the fact that the H and LE observations are higher on average with the reduced dataset, and hence with minor changes in rmsd values this results in generally smaller mapd values. With the full dataset, the average observed H and LE are about 170 and 230 $W m^{-2}$, respectively, while with the reduced dataset the averages are about 200 and 265 $W m^{-2}$.

5. Conclusions

The model proposed by Norman et al. (1995) for computing spatially distributed surface fluxes with radiometric surface temperature observations, $T_R(\phi)$, was applied to grass-covered surfaces of varying fractional cover and to bare soil. The model requires meteorological data, namely, wind speed, u , and air temperature, T_A , which ideally would be representative of the local field conditions. However, this information is not available on a regional basis, so observations higher up in the atmosphere, which are relatively uniform over the region, were used in model computations (i.e., in the mixed layer). By using the local roughness and vegetation information and the corresponding $T_R(\phi)$ observation for each site with the mixed-layer potential temperature, Θ_M , and wind speed, U_M , in the model, this resembles the so-called tile or mosaic approach (e.g., Koster and Suarez 1992) and is also similar to the flux-

aggregation method of using meteorological data at the blending height (Claussen 1991).

Four versions of the model were tested (see Table 2). The best agreement between modeled and observed H and LE fluxes come from using the local u and T_A observations (i.e., N95_L version) where mapd values were on the order of 20%–25%. Model performance deteriorated somewhat, which yielded mapd values on the order of 30%–35%, on average, and generally larger rmsd values when Θ_M and U_M were used in similarity approaches (i.e., model versions N95_{BL}, N95_{SL}, and N95_{SB}). Model performance was particularly poor when Θ_M and U_M were used with a regional roughness, Z_{OM} , and stability formulas [cf. Eqs. (7a) and (7b)] proposed by Sugita and Brutsaert (1992), N95_{SB}. The increase in mapd values for H and LE with N95_{BL} and N95_{SL} was mainly caused by larger biases between modeled and observed fluxes for some of the sites, while the N95_{SB} model also predicted significantly more variation in the heat fluxes.

Although there was a slight reduction in model performance, these results indicate that bulk similarity approaches as used by N95_{BL} and N95_{SL} model versions with high-resolution $T_R(\phi)$ data may compute spatially distributed fluxes without incurring a significant increase in error for type A surfaces (Shuttleworth 1988). Such $T_R(\phi)$ data will be available in 1999 from the ASTER instrument on the EOS AM-1 satellite platform. This would be a much simpler approach than trying to estimate u and T_A for each pixel value of $T_R(\phi)$ (e.g., Gao 1995). This tile or mosaic approach is also implicit in several SVAT models that use remote sensing data (Gillies and Carlson 1995; Gillies et al. 1997; Anderson et al. 1997). From these studies, comparisons between SVAT predictions of the heat fluxes with micrometeorological observations yielded similar results to the present study.

The results from this study also suggest that in the application of bulk similarity approaches with Θ_M and U_M for this surface type, it is more appropriate to define the local roughness, z_{OM} , for each elemental area representative of the corresponding $T_R(\phi)$ observation than to use regional roughness formulations, such as the one suggested by Sugita and Brutsaert (1992). Although Sugita and Brutsaert's bulk similarity approach is theoretically sound because the formulations were obtained by matching the inner or surface layer with the outer or mixed layer region of the ABL, using a regional scale estimate of R_A with $T_R(\phi)$ observations representative of local conditions is not appropriate. This mismatch in scale may be alleviated somewhat by using the local roughness z_{OM} , which then provides a more representative R_A that is used in predicting wind speed just above the canopy and soil surfaces of each elemental area. For many SVAT models and for N95 in particular, this local wind speed can significantly influence the resistance to heat transfer from the soil and canopy surfaces and, in turn, affect the heat flux predictions (see the appendix).

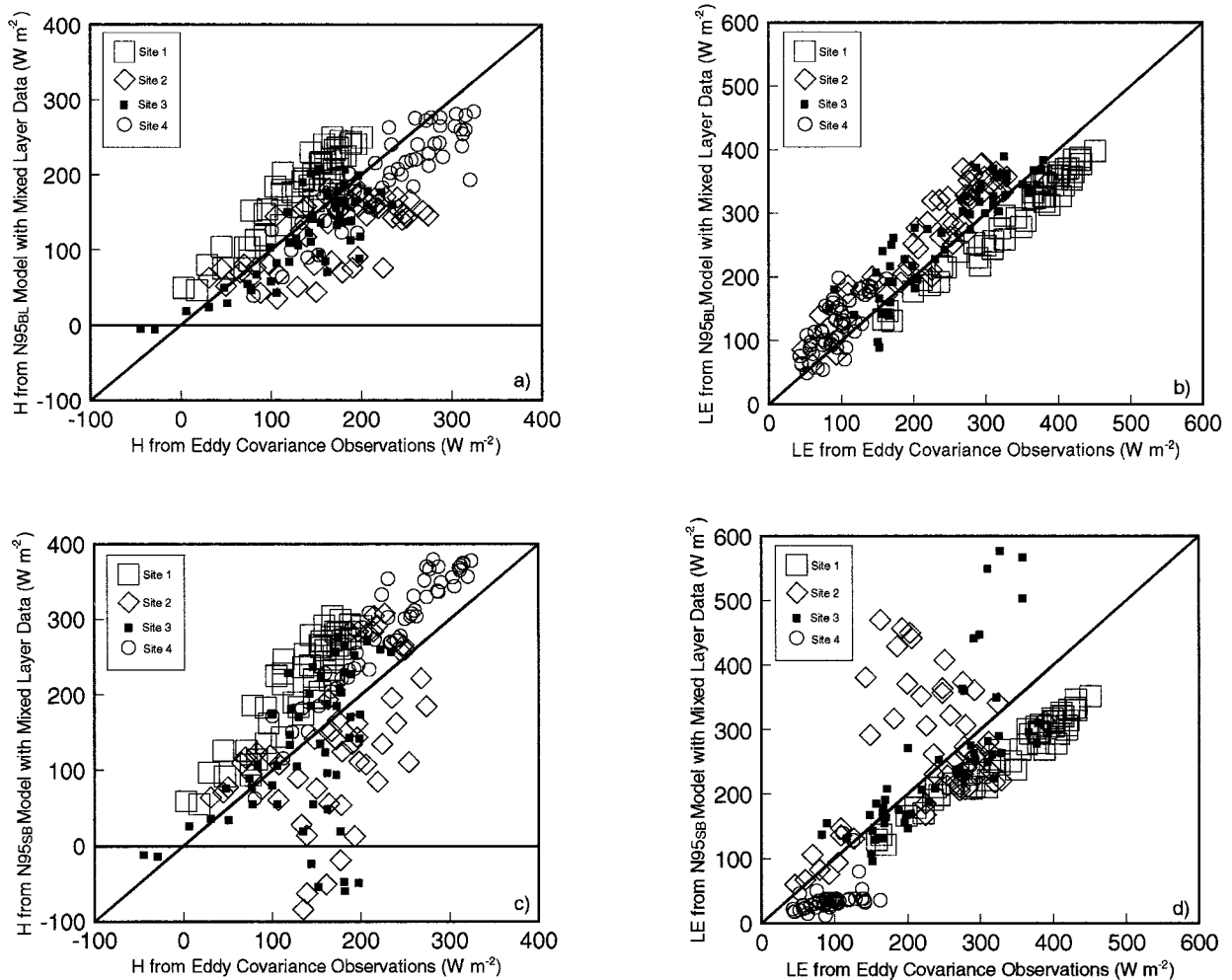


FIG. 2. A comparison of N95_{BL} model-predicted heat fluxes vs observed (a) H and (b) LE and N95_{SB} model-predicted heat fluxes vs observed (c) H and (d) LE from the four METFLUX sites. See text and Table 2 for descriptions of the N95_{BL} and N95_{SB} model versions. The line represents perfect agreement.

Therefore, Sugita and Brutsaert's approach requires the pixel size of $T_R(\phi)$ observations to be commensurate with the length scales representative of the regional roughness (e.g., Sugita et al. 1997).

While there are numerous studies that have evaluated local roughness z_{OM} from various surfaces, there are relatively few estimates of regional scale roughness (Parlange et al. 1995). Unfortunately, determining regional or effective roughness values from aggregating z_{OM} values based on land cover information is prone to significant error (Klassen and Claussen 1995). A possible solution to this problem is in the application of the present technique using U_M and Θ_M with high-resolution remote sensing data, such as from the ASTER instrument. Since heat fluxes aggregate linearly (Rau-pach and Finnigan 1995), the local spatially distributed fluxes derived by the model could be averaged for the whole image (for ASTER this would be $65 \text{ km} \times 65 \text{ km}$), thereby providing more reliable regional scale flux

estimates. This information could, in turn, be used to develop better techniques to determine the effective roughness parameters that are more appropriate with approaches similar to Sugita and Brutsaert's that are applied to much coarser resolution data such as GOES.

In future work, comparisons need to be made between approaches similar to Gao (1995) using local meteorological data derived from remotely sensed data (Gao et al. 1998) and the techniques using mixed-layer observations described in this paper. Future investigations are planned for exploring factors contributing to the increase biases between modeled and observed fluxes when using bulk similarity formulations.

Acknowledgments. The authors would like to thank Drs. Frank R. Schiebe (retired) and Thomas J. Jackson of the USDA-ARS and Dr. Edwin T. Engman of NASA for their cooperation and assistance in making this experiment possible. In addition, we would like to thank

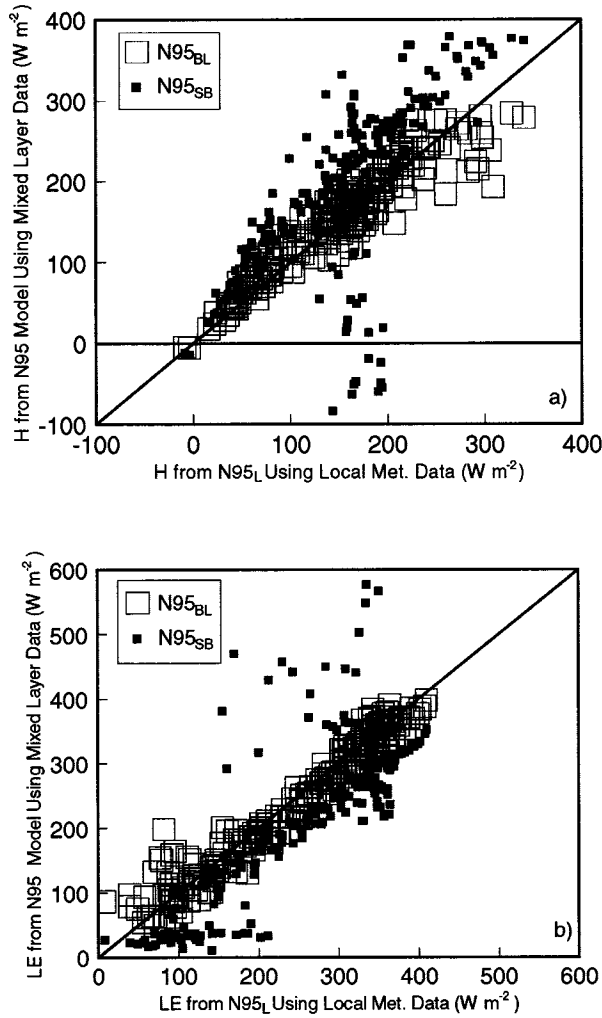


FIG. 3. A comparison of N95_L model heat flux predictions of (a) H and (b) LE vs N95_{BL} and N95_{BS} model predictions. See text and Table 2 for descriptions of the N95_L, N95_{BL}, and N95_{SB} model versions. Symbols are not used to distinguish heat flux predictions from the four METFLUX sites. The line represents perfect agreement.

the personnel at the USDA-ARS Little Washita River Watershed Field Office in Chickasha, especially Gary Heathman, for handling much of the logistics during the field campaign. The authors are also greatly indebted to the sounding team, Drs. Conrad L. Ziegler and Lester C. Showell from the National Severe Storms Laboratory (NSSL) and Dr. Christa Peters-Lidard now at the Georgia Institute of Technology, whose dedicated efforts provided consistent and reliable upper-air data and to the technical support provided by the In-Situ Observing Systems Group at NSSL. Comments by Drs. Jerry Hatfield, Randal Koster, and Larry Mahrt on earlier versions of this manuscript and comments made by the anonymous reviewers are greatly appreciated. Major funding in support of many of the data collection activities were provided by NASA and USDA-ARS.

APPENDIX

Overview of N95 Model

With the use of a single emissivity to represent the combined soil and vegetation the ensemble directional radiometric temperature $T_r(\phi)$ is related to the fraction of the radiometer view occupied by soil versus vegetation expressed as

$$T_r(\phi) \approx \{f(\phi) T_c^n + [1 - f(\phi)] T_s^n\}^{1/n}, \quad (\text{A1})$$

where T_c and T_s are the thermodynamic temperatures of the vegetation canopy and soil surface, respectively, and are assumed to represent spatially weighted averages of the sunlit and shaded portions of the canopy and soil, respectively, and $n \sim 4$. The fraction of the field of view of the infrared radiometer occupied by canopy, $f(\phi)$, depends upon the view zenith angle, ϕ , canopy type, and fraction of vegetative cover, f_c . For many vegetated surfaces, assuming a random canopy with a spherical leaf angle distribution is reasonable so that,

$$f(\phi) = 1 - \exp\left(\frac{-0.5LAI}{\cos\phi}\right). \quad (\text{A2})$$

The use of $T_r(\phi)$ frequently involves the controversial assumption that it is equivalent to the so-called aerodynamic temperature, T_o , of the surface. Here, T_o is the temperature that satisfies the bulk transport expression having the form

$$H = \rho C_p \frac{(T_o - T_A)}{R_{AH}}, \quad (\text{A3})$$

where H is the sensible heat flux (W m^{-2}), ρC_p is the volumetric heat capacity of air ($\text{J m}^{-3} \text{K}^{-1}$), T_A is the air temperature at some reference height above the surface (K), and R_{AH} is the resistance to heat transport (s m^{-1}), which has the following form in the surface layer (Brutsaert 1982):

$$R_{AH} = \frac{\left[\ln\left(\frac{z_U - d_o}{z_{OM}}\right) - \Psi_M \right] \left[\ln\left(\frac{z_T - d_o}{z_{OH}}\right) - \Psi_H \right]}{k^2 u}. \quad (\text{A4})$$

In this equation d_o is the displacement height (m); u is the wind speed (m s^{-1}) measured at height z_U (m); k is von Kármán's constant (≈ 0.4); z_T is the height (m) of the T_A measurement; Ψ_M and Ψ_H are the Monin-Obukhov stability functions for momentum and heat, respectively, and are functions of $(z - d_o)/L$ (see Brutsaert 1982), where $L = -u_*^3/[k(g/T_A)(H_v/\rho C_p)]$ is the Monin-Obukhov length (m), u_* is the friction velocity (m s^{-1}), g is the acceleration of gravity (m s^{-2}), $H_v = (H + 0.61T_A C_p E)$ is the virtual sensible heat flux (W m^{-2}), and E is the rate of surface evaporation ($\text{kg m}^{-2} \text{s}^{-1}$). The roughness parameter z_{OM} is the local roughness length (m) for momentum transport and z_{OH} is the local roughness length (m) for heat transport. Here, T_o cannot

be measured, so it is often replaced with an observation of $T_R(\phi)$ in Eq. (A3).

The net energy balance of the soil–canopy system is given by (neglecting photosynthesis)

$$R_N = H + LE + G. \quad (\text{A5})$$

The system of equations for computing fluxes from the soil and canopy components, denoted by subscripts s and c , respectively, are listed below and will be used by all versions of the model. The energy budgets for the soil and vegetation are given by

$$R_{N,S} = H_s + LE_s + G \quad (\text{A6})$$

$$R_{N,C} = H_c + LE_c, \quad (\text{A7})$$

with $R_N = R_{N,S} + R_{N,C}$. Similar to Eq. (A1) for estimating the contribution of soil and canopy temperatures to the observed radiometric temperature, Eqs. (2a) and (2b) are used for partitioning net radiation, R_N , between the soil and vegetation in order to properly weight the contributions of sensible, H , and latent heat flux, LE , from the soil and vegetation and estimate the soil heat flux G .

With $H = H_s + H_c$ and with the soil and vegetation taken in parallel (i.e., the resistance network provides for no interaction between the soil and vegetation), the heat fluxes from the soil and vegetation are computed by

$$H_s = \rho C_p \frac{T_s - T_A}{R_{AH} + R_s} \quad (\text{A8})$$

and

$$H_c = \rho C_p \frac{T_c - T_A}{R_{AH}}. \quad (\text{A9})$$

When H_c and H_s are taken in series (i.e., the resistance network allows for interaction between the soil and vegetation), then

$$H_s = \rho C_p \frac{T_s - T_{AC}}{R_s} \quad (\text{A10})$$

and

$$H_c = \rho C_p \frac{T_c - T_{AC}}{R_x}, \quad (\text{A11})$$

where T_{AC} is related to T_o in Eq. (A3), namely,

$$H = \rho C_p \frac{T_{AC} - T_A}{R_A}. \quad (\text{A12})$$

See Figs. 1 and 11 in N95 illustrating the parallel and series resistance network.

Finally, for $LE = LE_s + LE_c$ the fluxes are estimated by the following expressions:

$$LE_s = R_{N,S} - G - H_s \quad (\text{A13})$$

and

$$LE_c = \alpha_{PT} f_G \frac{\Delta}{\Delta + \gamma} R_{N,C}, \quad (\text{A14})$$

where G is simply taken as a fraction of $R_{N,S}$ via Eq. (3) with c_G estimated from Eq. (4).

Here, R_s is the resistance to heat flow in the boundary layer immediately above the soil surface and is estimated from an empirical expression developed by Sauer et al. (1995), and R_x is the total boundary layer resistance of the complete canopy of leaves (see appendix A in N95) estimated with the wind speed in the canopy air space computed from the equations of Goudriaan (1977). Here, R_{AH} is estimated using Eq. (A4) with local d_o and z_{OM} estimated as a fraction of canopy height, h_c , [i.e., $d_o \approx 0.65 h_c$; $z_{OM} \approx 0.13 h_c$; see Brutsaert (1982)] and z_{OH} is estimated as a fraction of z_{OM} as postulated by Garratt and Hicks (1973), namely, $z_{OH} \approx z_{OM}/7$ or $\text{kB}^{-1} \approx 2$; however, recent evidence suggests that z_{OH} probably is related to canopy characteristics (McNaughton and Van den Hurk 1995). Here, R_A is computed from Eq. (A4) with $z_{OH} = z_{OM}$. The term T_{AC} is the momentum aerodynamic temperature and only approximates the temperature in the canopy air space (see appendix A in N95). The Priestley–Taylor parameter α_{PT} is set equal to 1.26 (Priestley and Taylor 1972) for the green part of the canopy, Δ is the slope of the saturation vapor pressure–temperature curve (Pa K^{-1}), and γ is the psychrometric constant ($\approx 66 \text{ Pa K}^{-1}$). The fraction of LAI that is “green” or actively transpiring, f_G , may be obtained from knowledge of the phenology of the vegetation. If no information is available for estimating f_G , then it is assumed to equal unity.

Equation (A14) only provides an initial calculation of LE_c , and it can be overridden if the temperature difference between the soil–canopy system and the atmosphere is large causing erroneous flux estimates, such as negative LE_s or condensation during the daytime period. If the estimated radiometric temperature from Eq. (A1) is less than the measured $T_R(\phi)$, then the Priestley–Taylor approximation in Eq. (A14) will tend to overestimate the canopy transpiration rate because the water supply in the root zone is inadequate. Therefore an iteration procedure will compute LE_c values below estimates given by Eq. (A14) until values of T_c and T_s used in Eq. (A1) agree with the measured $T_R(\phi)$. Further details concerning model convergence issues for the energy budgets of the soil and vegetation in later iterations and the justification for the Priestley–Taylor assumption used in Eq. (A14) are given in N95.

REFERENCES

- Allen, P. B., and J. W. Naney, 1991: Hydrology of the Little Washita River Watershed, Oklahoma. Data and analyses. Tech. Rep. ARS-90, U.S. Dept. of Agriculture, Agricultural Research Service Durant, OK, 74 pp. [Available from National Technical Information Service, 5285 Port Royal Road, Springfield, VA 22161.]
- Anderson, M. C., J. M. Norman, G. R. Diak, W. P. Kustas, and J. R. Mecikalski, 1997: A two-source time-integrated model for estimating surface fluxes from thermal infrared satellite observations. *Remote Sens. Environ.*, **60**, 195–216.
- Avisar, R., and R. A. Pielke, 1989: A parameterization of hetero-

- geneous land surfaces for atmospheric numerical models and its impact on regional meteorology. *Mon. Wea. Rev.*, **117**, 2113–2136.
- Beljaars, A. C. M., 1995: The parameterization of surface fluxes in large scale models under free convection. *Quart. J. Roy. Meteor. Soc.*, **121**, 255–270.
- Blyth, E. M., 1995: Using a simple SVAT scheme to describe the effect of scale aggregation. *Bound.-Layer Meteor.*, **72**, 267–285.
- , A. J. Dolman, and N. Wood, 1993: Effective resistance to sensible and latent heat flux in heterogeneous terrain. *Quart. J. Roy. Meteor. Soc.*, **119**, 423–442.
- Brutsaert, W., 1982: *Evaporation into the Atmosphere*. D. Reidel, 299 pp.
- , 1992: Stability correction functions for the mean wind speed and temperature in the unstable surface layer. *Geophys. Res. Lett.*, **19**, 469–472.
- , and M. Sugita, 1991: A bulk similarity approach in the atmospheric boundary layer using radiometric skin temperature to determine regional surface fluxes. *Bound.-Layer Meteor.*, **55**, 1–23.
- , and M. B. Parlange, 1996: The relative merits of surface layer and bulk similarity formulations of shear stress. *J. Geophys. Res.*, **101** (D23), 29 585–29 589.
- Choudhury, B. J., 1987: Relationships between vegetation indices, radiation absorption, and net photosynthesis evaluated by a sensitivity analysis. *Remote Sens. Environ.*, **22**, 209–233.
- , N. U. Ahmed, S. B. Idso, R. R. Reginato, and G. S. T. Daughtry, 1994: Relations between evaporation coefficients and vegetation indices studied by model simulations. *Remote Sens. Environ.*, **50**, 1–17.
- Claussen, M., 1991: Estimation of areally-averaged surface fluxes. *Bound.-Layer Meteor.*, **54**, 387–410.
- , 1995: Flux aggregation at large scales: On the limits of validity of the concept of blending height. *J. Hydrol.*, **166**, 371–382.
- Dugas, W. A., L. J. Fritschen, L. W. Gay, A. A. Held, A. D. Matthias, D. C. Reicosky, P. Steduto, and J. L. Steiner, 1991: Bowen ratio, eddy correlation, and portable chamber measurements of sensible and latent heat flux over irrigated spring wheat. *Agric. For. Meteorol.*, **56**, 1–20.
- Friedl, M. A., 1996: Relationships among remotely sensed data, surface energy balance, and area-averaged fluxes over partially vegetated land surfaces. *J. Appl. Meteorol.*, **35**, 2091–2103.
- Fritschen, L. J., P. Qian, E. T. Kanemasu, D. Nie, E. A. Smith, J. B. Stewart, S. B. Verma, and M. L. Wesely, 1992: Comparisons of surface flux measurement systems used in FIFE 1989. *J. Geophys. Res.*, **97** (D17), 18 697–18 713.
- Gao, W., 1995: Parameterization of subgrid-scale land surface fluxes with emphasis on distributing mean atmospheric forcing and using satellite-derived vegetation index. *J. Geophys. Res.*, **100** (D7), 14 305–14 317.
- , R. L. Coulter, B. M. Lesht, J. Qiu, and M. L. Wesely, 1998: Estimating clear-sky regional surface fluxes in the Southern Great Plains atmospheric radiation measurement site with ground measurements and satellite observations. *J. Appl. Meteorol.*, **37**, 5–22.
- Garratt, J. R., and B. B. Hicks, 1973: Momentum, heat and water vapor transfer to and from natural and artificial surfaces. *Quart. J. Roy. Meteor. Soc.*, **99**, 680–687.
- Gillies, R. R., and T. N. Carlson, 1995: Thermal remote sensing of surface soil water content with partial vegetation cover for incorporation into climate models. *J. Appl. Meteorol.*, **34**, 745–756.
- , J. Cui, W. P. Kustas, and K. S. Humes, 1997: A verification of the “triangle” method for obtaining surface soil water content and energy fluxes from remote measurements of the normalized difference vegetation index (NDVI) and surface radiant temperature. *Int. J. Remote Sens.*, **18**, 3145–3166.
- Goudriaan, J., 1977: *Crop Micrometeorology: A Simulation Study*. Centre for Agricultural Publishing and Documentation, Wageningen, the Netherlands, 249 pp.
- Hechtel, L. M., C.-H. Moeng, and R. B. Stull, 1990: The effects of nonhomogeneous surface fluxes on the convective boundary layer: A case study using large-eddy simulation. *J. Atmos. Sci.*, **47**, 1721–1741.
- Kizer, M. A., and R. L. Elliott, 1991: Eddy correlation systems for measuring evapotranspiration. *Trans. Amer. Soc. Agric. Eng.*, **34**, 387–392.
- Klassen, W., and M. Claussen, 1995: Landscape variability and surface flux parameterization in climate models. *Agric. For. Meteorol.*, **73**, 181–188.
- Koster, R., and M. Suarez, 1992: A comparative analysis of two land surface heterogeneity representations. *J. Climate*, **5**, 1379–1390.
- Kustas, W. P., and C. S. T. Daughtry, 1990: Estimation of the soil heat flux/net radiation ratio from spectral data. *Agric. For. Meteorol.*, **49**, 205–223.
- , and K. S. Humes, 1996: Variations in the surface energy balance for a semi-arid rangeland using remotely sensed data at different spatial resolutions. *The Scaling Issue in Hydrology*, J. B. Stewart, and Coeditors, John Wiley and Sons, 127–145.
- , and J. M. Norman, 1997: A two-source approach for estimating turbulent fluxes using multiple angle thermal infrared observations. *Water Resour. Res.*, **33**, 1495–1508.
- , L. E. Hippias, and K. S. Humes, 1995: Calculation of basin-scale surface fluxes by combining remotely sensed data and atmospheric properties in a semiarid landscape. *Bound.-Layer Meteorol.*, **73**, 105–124.
- , X. Zhan, and T. J. Schmugge, 1998: Combining optical and microwave remote sensing for mapping energy fluxes in a semi-arid watershed. *Remote Sens. Environ.*, **64**, 116–131.
- Mahrt, L., 1996: The bulk aerodynamic formulation over heterogeneous surfaces. *Bound.-Layer Meteorol.*, **78**, 87–119.
- , and J. Sun, 1995: Dependence of surface exchange coefficients on averaging scale and grid size. *Quart. J. Roy. Meteor. Soc.*, **121**, 1835–1852.
- Mason, P. J., 1988: The formation of areally-averaged roughness lengths. *Quart. J. Roy. Meteor. Soc.*, **114**, 399–420.
- McNaughton, K. G., and B. J. J. M. Van den Jurk, 1995: A “Lagrangian” revision of the resistors in the two-layer model for calculating the energy budget of a plant canopy. *Bound.-Layer Meteorol.*, **74**, 262–288.
- Moran, M. S., W. P. Kustas, A. Vidal, D. I. Stannard, J. H. Blanford, and W. D. Nichols, 1994: Use of ground-based remotely sensed data for surface energy balance evaluation of a semiarid rangeland. *Water Resour. Res.*, **30**, 1339–1349.
- Nie, D., and Coauthors, 1992: An intercomparison of surface energy flux measurement systems used during FIFE 1987. *J. Geophys. Res.*, **97** (D17), 18 715–18 724.
- Norman, J. M., and G. S. Campbell, 1983: Application of a plant-environment model to problems in irrigation. *Advances in Irrigation*, D. I. Hillel, Ed., Academic Press, 155–188.
- , W. P. Kustas, and K. S. Humes, 1995: A two-source approach for estimating soil and vegetation energy fluxes from observations of directional radiometric surface temperature. *Agric. For. Meteorol.*, **77**, 263–293.
- Parlange, M. B., W. E. Eichinger, and J. D. Albertson, 1995: Regional scale evaporation and the atmospheric boundary layer. *Rev. Geophys.*, **33**, 99–124.
- Priestly, C. H. B., and R. J. Taylor, 1972: On the assessment of surface heat flux and evaporation using large-scale parameters. *Mon. Wea. Rev.*, **100**, 81–92.
- Prueger, J. H., J. L. Hatfield, W. P. Kustas, and K. S. Humes, 1996a: Micrometeorological measurements. *Hydrology Data Report Washita '94*, P. J. Starks and K. S. Humes, Eds., USDA-ARS NAWQL 96-1, X(1)–X(15).
- , W. P. Kustas, J. L. Hatfield, K. S. Humes, and T. J. Sauer, 1996b: Surface energy partitioning in the Little Washita during 1994. *Proc. 22d Conf. on Agricultural and Forest Meteorology with Symp. on Fire and Forest Meteorology and 12th Conf. on Biometeorology and Aerobiology*, Atlanta, GA, Amer. Meteor. Soc., J89–J90.
- Qualls, R. J., and W. Brutsaert, 1996: Evaluation of spatially distrib-

- uted ground-based and remotely sensed data to estimate spatially distributed sensible heat fluxes. *Water Resour. Res.*, **32**, 2489–2495.
- Raupach, M. R., and J. J. Finnigan, 1995: Scale issues in boundary-layer meteorology: Surface energy balances in heterogeneous terrain. *Hydrol. Processes*, **9**, 589–612.
- Ross, J., 1975: Radiative transfer in plant communities. *Vegetation and the Atmosphere*, J. L. Monteith, Ed., Academic Press, 13–55.
- , 1981: *The Radiation Regime and Architecture of Plant Stands*. Tasks for Vegetation Sciences, Vol. 3, Dr. W. Junk Publishers, 391 pp.
- Rust, W. D., R. P. Davies-Jones, D. W. Burgess, R. A. Maddox, L. C. Showell, T. C. Marshall, and D. K. Lauritsen, 1990: Testing a mobile version of a cross-chain Loran atmospheric sounding system (M-CLASS). *Bull. Amer. Meteor. Soc.*, **71**, 173–180.
- Sauer, T. J., J. M. Norman, C. B. Tanner, and T. B. Wilson, 1995: Measurement of heat and vapor transfer at the soil surface beneath a maize canopy using source plates. *Agric. For. Meteorol.*, **75**, 161–189.
- Schuepp, P. H., M. Y. Lecler, J. I. Macpherson, and R. L. Desjardins, 1990: Footprint prediction of scalar fluxes from analytical solution of the diffusion equation. *Bound.-Layer Meteorol.*, **50**, 355–373.
- Seth, A., F. Giorgi, and R. E. Dickenson, 1994: Simulating fluxes from heterogeneous land surfaces: Explicit subgrid method employing the biosphere–atmosphere transfer scheme (BATS). *J. Geophys. Res.*, **99**, 18 651–18 667.
- Shuttleworth, W. J., 1988: Macrohydrology—The new challenge for process hydrology. *J. Hydrol.*, **100**, 31–56.
- Stannard, D. I., J. H. Blanford, W. P. Kustas, W. D. Nichols, S. A. Amer, T. J. Schmugge, and M. A. Weltz, 1994: Interpretation of surface flux measurements in heterogeneous terrain during the Monsoon '90 experiment. *Water Resour. Res.*, **30**, 1227–1239.
- Starks, P. J., and K. S. Humes, 1996: *Hydrology Data Report Washita '94*. USDA-ARS NAWQL, 179 pp.
- Stull, R. B., and E. W. Eloranta, 1984: Boundary layer experiment 1983. *Bull. Amer. Meteor. Soc.*, **65**, 450–456.
- Sugita, M., and W. Brutsaert, 1992: The stability functions in the bulk similarity formulation for the unstable boundary layer. *Bound.-Layer Meteorol.*, **61**, 65–80.
- , T. Hiyama, and I. Kayane, 1997: How regional are the regional fluxes obtained from lower atmospheric boundary layer data? *Water Resour. Res.*, **33**, 1437–1445.
- Tsu, H., Y. Yamaguchi, and A. B. Kahle, 1996: ASTER science mission overview. *Proc. SPIE-Int. Soc. Opt. Eng. Infrared Spaceborne Remote Sensing*, **2817**, 52–59.
- Willmott, C. J., 1982: Some comments on the evaluation of model performance. *Bull. Amer. Meteor. Soc.*, **63**, 1309–1313.
- Zhan, X., W. P. Kustas, and K. S. Humes, 1996: An intercomparison study on models of sensible heat flux over partial canopy surfaces with remotely sensed surface temperature. *Remote Sens. Environ.*, **58**, 242–256.
- Ziegler, C. L., and L. C. Showell, 1996: Atmospheric soundings. *Hydrology Data Report Washita '94*, P. J. Starks and K. S. Humes, Eds., USDA-ARS NAWQL 96-1, XII(1)–XII(15).